Chen-Hu, K., Fernandez-Getino, M. J. , Tonello, A. M. & Garcia, A. (2021). Low-Complexity Power Allocation in Pilot-Pouring Superimposed-Training Over CB-FMT. *IEEE Transactions on Vehicular Technology, 70*(12), 13010–13021.

DOI: 10.1109/tvt.2021.3123389

Low-Complexity Power Allocation in Pilot-Pouring Superimposed-Training over CB-FMT

Kun Chen-Hu, *Member, IEEE,* M. Julia Fernández-Getino García, *Member, IEEE*, Andrea M. Tonello, *Senior Member, IEEE*, and Ana García Armada, *Senior Member, IEEE*

***Abstract*—Pilot-pouring superimposed training (PPST) is a novel channel estimation technique specially designed for cyclic block filtered multi-tone (CB-FMT), where the pilot symbols are poured into the subcarriers taking advantage of the power left unused by the data symbols. Hence, since this technique is based on superimposed training (ST) principles, the data rate is not reduced, unlike the pilot symbol assisted modulation (PSAM). Besides, it exploits a weighted average at the receiver side that is capable of minimizing the mean squared error (MSE) of the channel estimation, and then enhancing the performance of the system. However, the existing proposal on PPST is limited to the minimization of the MSE to improve channel estimation for a given power allocation factor, without solving the joint optimization of channel estimation and data detection procedures. With this aim, this work addresses the whole problem to reach the best performance for both tasks, thus taking into account also the power allocation factor in the optimization process, where the spectral efficiency must be maximized through the signal-to-interference plus noise ratio (SINR). Two optimization approaches are proposed, where the first one, referred as pilot-pouring optimization (PPO), is focused on performance at the expense of a high complexity, while the second one, denoted as low-complexity PPO (LPPO), is able to trade-off between performance and execution time. Numerical results are provided in order to show the validity of our proposal, where the different optimization problems are compared in terms of SINR and execution time.**

***Index Terms*—5G, FMT, channel estimation, multicarrier modulation, superimposed training, pilot-pouring.**

I. Introduction

ORTHOGONAL frequency division multiplexing (OFDM) [1], [2] has been widely adopted as the waveform for several communication standards, such as Fourth and Fifth Generation of mobile communication system (4G [3] and 5G [4]). It can be efficiently implemented by a fast-Fourier transform (FFT), and the insertion of the cyclic prefix (CP) allows to avoid the inter-symbol and inter-carrier interference, and thus, enabling a low-complexity one-tap equalizer. However, these benefits come at the expense of exhibiting a high peak-to-average power ratio (PAPR) and increased out-of-band emissions due to the use of a rectangular pulse shape. Alternatively, different waveform candidates based on filtered multi-tone (FMT) modulation [5] haven also been proposed by the scientific community, where a better frequency confinement can be obtained by exploiting well-localized prototype filters in the frequency dimension, and hereby, making a better use of the available spectrum. The different waveforms proposed are filter-bank multi-carrier (FBMC) [6], [7], universal filtered multi-carrier (UFMC) [8], generalized frequency division multiplexing (GFDM) [9] and cyclic block FMT (CB-FMT) [10]–[12]. Recently, CB-FMT has been considered an appealing technique to replace the well-known OFDM due to the fact that it possesses a similar architecture to single-carrier frequency-division multiple access (SC-FDMA) [3], [4], and therefore, the backward and forward compatibility can be ensured. Besides, it is also capable of reducing the PAPR as compared to OFDM and keeping the orthogonality among subcarriers.

The performance evaluation of these waveforms is typically performed under the assumption that the channel state information (CSI) is perfectly acquired by any existing technique developed for OFDM, such as pilot symbol assisted modulation (PSAM) [13]. However, it causes an additional overhead produced by transmitting some reference signals. Besides, this data-rate reduction can be enhanced further in those waveforms based on splitting the frequency resources into several independently processed sub-channels, such as SC-FDMA, UFMC, GFDM and CB-FMT, where an entire sub-channel must be exclusively allocated for transmitting either data or pilot symbols. For example, a resource block (RB) is a sub-channel of twelve contiguous subcarriers in 4G [3] and 5G [4], and the reference symbols are allocated to an entire RB for the above waveforms, while OFDM may only require one or two subcarriers on each RB.

Superimposed training (ST) has been recently combined with different waveforms since it is able to avoid the data-rate loss induced by PSAM and provides a good trade-off between complexity and performance. Each time-frequency resource is shared by data and pilot symbols with their own allocated power, and therefore, the efficiency of the system is increased at the expense of adding an additional interference produced by the superimposed data symbols, as compared to PSAM. Typically, acceptable CSI can be obtained by using an arithmetic averaging, that is able to minimize the interference

Kun Chen-Hu, M. Julia Fernández-Getino García and Ana García Armada are with the Department of Signal Theory and Communications of Carlos III University of Madrid, Leganés, 28911, Spain. E-mails: {kchen, mjulia, agarcia}@tsc.uc3m.es.

Andrea M. Tonello is with the Institute of Networked and Embedded Systems, University of Klagenfurt, 9020 Klagenfurt, Austria. E-mail: andrea.tonello@aau.at.

This work has been partially funded by the Spanish National projects TERESA-ADA (TEC2017-90093-C3-2-R) (MINECO/AEI/FEDER, UE) and IRENE-EARTH (PID2020-115323RB-C33 / AEI / 10.13039/501100011033), and the work of A. M. Tonello has been supported in part by the Chair of Excellence Program of the Universidad Carlos III de Madrid.

produced by the superimposed data symbols and noise effects. ST combined with OFDM was proposed in [14] assuming that all subcarriers have the same allocated power. It was shown that the overall capacity of the system using ST is higher than with PSAM, when a sufficient number of consecutive OFDM symbols is available for the averaging. The optimum percentage of power allocated to data and pilot symbols is obtained for each signal-to-noise ratio (SNR) value. ST combined with FBMC was analysed in [15], [16], pointing out that this combination has an even better performance, as compared to the OFDM case given in [14], due to the fact that not only FBMC does not make use of CP, but also the averaging process can also filter out the intrinsic data-interference produced by the loss of orthogonality. Partial data ST (PDST) was introduced in [17], where the power allocated to the data and pilot symbols at each subcarrier is different to others. Particularly, the pilot symbols are only superimposed at some specific subcarriers, unlike the classical ST [14], leaving other resources for the exclusive transmission of data symbols. Hence, this hybrid proposal is capable of exploiting the advantages of both PSAM and ST. Recently, pilot-pouring ST (PPST) combined with CB-FMT was presented in [18]. CB-FMT makes use of the well-localized prototype filters in the frequency domain for each sub-channel, where the frequency response of this filter allows to pour the data and pilot symbols power within the spectrum. As first approach, the power allocated to the superimposed pilot symbols in the spectrum corresponds to the power left unused by the data ones, guaranteeing that the whole power of data and poured pilot symbols is equally distributed to all subcarriers. Besides, at the receiver, a weighted average was proposed to smartly weight the received superimposed pilots according to the mean squared error (MSE) of the CSI [18].

PPST [18] can be seen as a generalization of the different existing ST techniques [14]–[17], where the pilot-pouring and the average coefficients have been particularized for some specific filter dependent values. However, the optimization problem provided in [18] was not properly characterized to obtain the best performance of PPST, due to the fact that it focused on reducing the channel estimation error instead of maximizing the signal to interference plus noise ratio (SINR), i.e. the spectral efficiency, without taking into account the power allocation factor. Also, there was another limitation since the optimization variables were constrained to guarantee that the power was equally distributed over all subcarriers. Hence, the provided numerical results may not correspond to the best choice since the complete optimization problem was unsolved. Therefore, the main contributions of this paper are the following:

- Given the PPST technique proposed in [18] and following [14]–[17], a pilot-pouring optimization (PPO) is proposed, that is designed to maximize the SINR of the system. No additional constraints are imposed to the three optimization variables (the power allocation factor, the pilot-pouring coefficients and the average coefficients) for a particular prototype filter.
- In order to increase the efficiency of the proposed optimization problem and without penalizing the performance, an alternative low-complexity PPO (LPPO) is also proposed, due to the fact that PPO is a non-convex optimization with respect to the weighted average coefficients. This second proposal splits the problem into three individual complex optimization problems, where each block is responsible for obtaining each optimization variable. The weighted average is constrained to an arithmetic one to reduce its complexity. Both the average and pilot-pouring coefficients are obtained by minimizing the MSE of the channel estimation error, and they can be efficiently implemented by exploiting an ordered search and the well-known Water-Filling method, respectively. Then, the power allocation factor can be obtained through maximizing the SINR by exploiting the bisection algorithm.
- Some numerical results in terms of SINR, execution time and spectral efficiency are shown for the different proposed approaches, highlighting that the PPO has the best performance at the expense of sacrificing the complexity. On the other hand, LPPO shows a very similar performance as compared to PPO and the execution time is dramatically reduced. Finally, a comparison in terms of spectral efficiency between the proposed PPST and the traditional PSAM is provided, where the former outperforms the latter for different configurations of reference signals deployed in 5G [4].

The remainder of the paper is organized as follows. Section II introduces the system model of PPST. Section III provides the description of the PPO problem capable of maximizing the SINR. Section IV proposes an alternative low-complexity PPO solution. Section V shows the numerical results for our proposed methods to provide a better understanding of the system. Finally, in Section VI, the conclusions follow.

Notation: matrices, vectors and scalar quantities are denoted by boldface uppercase, boldface lowercase, and normal letters, respectively. $[\mathbf{A}]_{m,n}$ denotes the element in the m-th row and n-th column of $\mathbf{A}$. $[\mathbf{a}]_n$ represents the n-th element of vector $\mathbf{a}$. $\circ$ is the Hadamard product of two matrices. $\mathbb{E}\{\cdot\}$ represents the expected value. $\mathcal{CN}(0,\sigma^2)$ represents the circularly-symmetric and zero-mean complex normal distribution with variance σ^2. $\max(\mathbf{a})$ corresponds to the maximum value of the vector $\mathbf{a}$.

II. System Model

The proposed system is a single-input single-output one. It is assumed that the transmitter sends N CB-FMT symbols of K orthogonal subcarriers. According to [10]–[12], the filter-bank can be efficiently implemented in the frequency domain, where the cyclic convolution is replaced by a dot product between data signals and the prototype pulse coefficients. As a consequence, CB-FMT can be synthesized by exploiting the well-known OFDM (inner inverse FFT (IFFT)) plus a bank of independent processing blocks (see Fig. 1). At the transmitter, each branch comprises a K_B-FFT (outer FFT) and a filtering. Later, the output of each branch is transmitted by using OFDM, where it is assumed that the CP is long enough

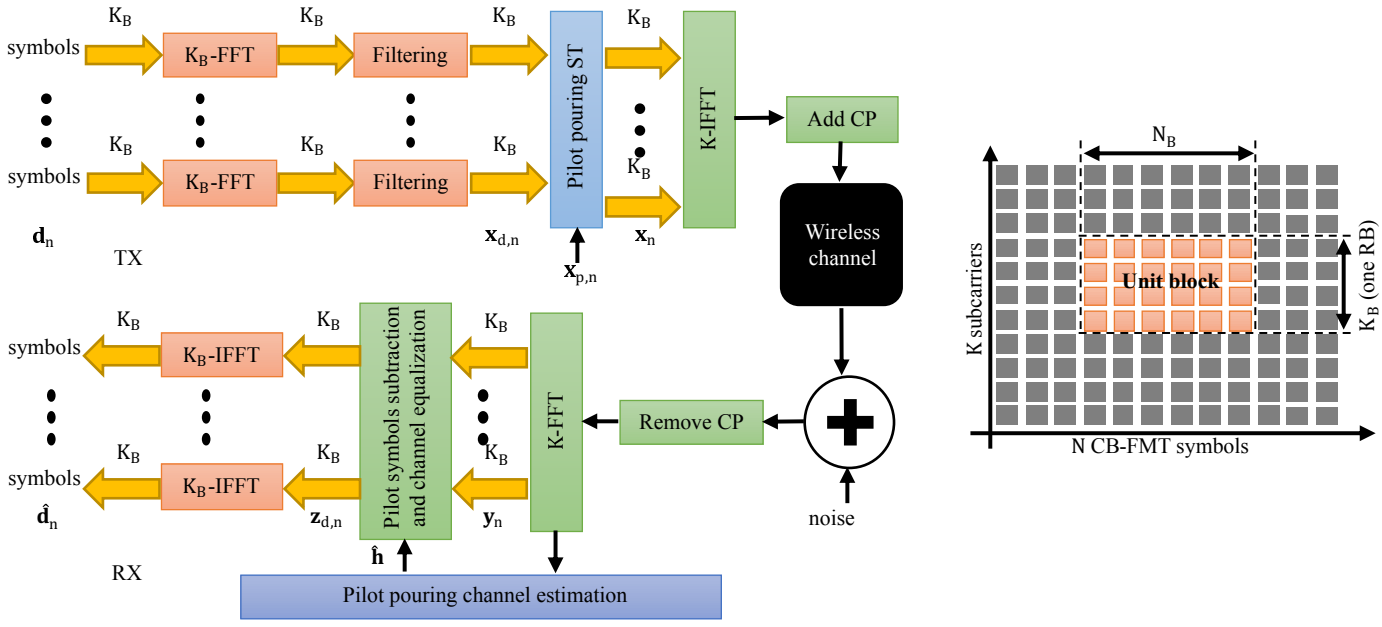

Fig. 1. Block diagram of CB-FMT with the pilot-pouring system (pilot insertion/removal, channel estimation and equalization), and definition of the unit block ($K_B \times N_B$)

to fully absorb the multiple paths of the channel. According to [18], the pilot insertion and the channel estimation are based on the pilot-pouring system, and they are performed at the OFDM level, see [10]–[12], [18].

Given the time-frequency resource grid, let us define the unit block which is a set of time-frequency resources built by K_B adjacent subcarriers and N_B contiguous CB-FMT symbols, which corresponds to the output of a particular processing branch (see Fig. 1). Moreover, following the notation of 4G [3] and 5G [4], let us define a RB as a set of K_B subcarriers, and hence, a unit block is built by N_B RBs. Without loss of generality and for the sake of easiness of notation, the analysis focuses on a particular unit block.

A. Transmitter: data processing and pilot-pouring

At the transmitter, the pre-processed data symbol vector $\mathbf{x}_{d,n}$ $(K_B \times 1)$ for a particular RB at n-th multi-carrier symbol can be obtained as

$$\mathbf{x}_{d,n} = \mathbf{g}_{d,n} \circ \mathbf{F}_{K_B}\mathbf{d}_n, \quad \mathbb{E}\left\{\|\mathbf{d}_n\|_F^2\right\} = 1, \quad \left\|\mathbf{g}_{d,n}\right\|_F^2 = 1, \quad (1)$$

$$\left[\mathbf{F}_{K_B}\right]_{a,b} = \frac{1}{\sqrt{K_B}} \exp\left(-j\frac{2\pi}{K_B}(a-1)(b-1)\right), \quad (2)$$
$$1 \le a, b \le K_B,$$

where $\mathbf{d}_n$ $(K_B \times 1)$ is the data symbol vector that belongs to a QAM constellation for the n-th CB-FMT symbol, $\mathbf{F}_{K_B}$ represents the FFT matrix operation, $\mathbf{g}_{d,n}$ $(K_B \times 1)$ corresponds to the coefficients of the frequency response of the prototype filter, which satisfy the symmetry condition, described as

$$\left[\mathbf{g}_{d,n}\right]_{a+1} = \left[\mathbf{g}_{d,n}\right]_{K_B-a}, \quad 0 \le a \le \frac{K_B}{2} - 1. \quad (3)$$

According to [10]–[12], the chosen prototype filter is typically well-localized in the frequency domain in order to reduce the out-of-band emissions and keep the orthogonality between unit blocks in the frequency domain. Hence, those coefficients of the frequency response of the prototype filter that correspond to the edge subcarriers of an unit block will be more attenuated with respect to the middle ones. This property will be exploited for the power allocation of the pilot symbols, in order to improve the channel estimation and, at the same time, keep the data rate as high as possible.

Then, the PPST is responsible for superimposing the pilot symbols over the pre-processed data ones, and hence, the complex symbol vector to be transmitted in one RB can be obtained as

$$\mathbf{x}_n = \sqrt{P_d}\mathbf{x}_{d,n} + \sqrt{P_p}\mathbf{x}_{p,n}, \quad 1 \le n \le N_B, \quad (4)$$

where $\mathbf{x}_{p,n}$ $(K_B \times 1)$ denotes the superimposed pilot symbol vector and P_d watt and P_p watt are the power allocated to data and pilot symbols, respectively. The pilot symbol vector is given by

$$\mathbf{x}_{p,n} = \mathbf{g}_{p,n} \circ \mathbf{p}_n, \quad \mathbb{E}\left\{\|\mathbf{p}_n\|_F^2\right\} = 1, \quad \left\|\mathbf{g}_{p,n}\right\|_F^2 = 1, \quad (5)$$

where $\mathbf{p}_n$ $(K_B \times 1)$ is the pilot sequence vector for the n-th CB-FMT symbol and $\mathbf{g}_{p,n}$ $(K_B \times 1)$ accounts for the pilot-pouring coefficients. Additionally, note that it must satisfy that

$$P_t = P_d + P_p, \quad P_d = (1-\beta)P_t, \quad P_p = \beta P_t, \quad 0 < \beta < 1, \quad (6)$$

where Pt watt is the total power available at the transmitter and β corresponds to the power allocation factor.

Finally, $\mathbf{x}_n$ is fed to the OFDM processing blocks, which are an IFFT of K subcarriers and a CP addition.

B. Receiver: channel estimation and data demodulation

A summary of channel estimation based on PPST and data detection operations for CB-FMT system is provided in this

sub-section. More details can be found in previous papers [14], [17], [18].

At the receiver, after removing the CP and performing the K-FFT, the received signal for a particular branch $\mathbf{y}_n$ $(K_B \times 1)$ can be described as

$$\mathbf{y}_n = \mathbf{h}_n \circ \mathbf{x}_n + \mathbf{v}_n, \quad 1 \leq n \leq N_B, \tag{7}$$

where $\mathbf{v}_n$ $(K_B \times 1)$ denotes the additive white Gaussian noise (AWGN) which is a vector of zero mean and variance σ_v^2 Gaussian components, and $\mathbf{h}_n$ $(K_B \times 1)$ is the frequency response of the multi-path channel vector at the n-th CB-FMT symbol, where each element follows a normal distribution with a zero mean and unit variance ($\sigma_h^2 = 1$).

In ST [14]–[17], averaging is required to filter out the self-interference produced by the data symbols and the noise. Following [18], in order to ease the notation and without loss of generality, the arithmetic and weighted averages in time and frequency dimensions, respectively, require that the chosen prototype filter and the pilot-pouring coefficients are fixed for the consecutive N_B CB-FMT symbols of the considered RB as

$$\mathbf{g}_{d,n} = \mathbf{g}_d, \quad \mathbf{g}_{p,n} = \mathbf{g}_p, \quad 1 \leq n \leq N_B. \tag{8}$$

Furthermore, in order to be able to perform the averaging in both time and frequency dimensions, the channel should remain quasi-static and the transmitted pilot symbols have the same value for those resources in the considered unit block. Hence, the channel frequency response and the pilots can be defined as

$$[\mathbf{h}_n]_k = h, \quad [\mathbf{p}_n]_k = p, \quad 1 \leq k \leq K_B, \quad 1 \leq n \leq N_B, \tag{9}$$

where h is the channel coefficient and p corresponds to the pilot symbol, which are the same values for the considered unit block.

Hence, the received signal after performing the first arithmetic average over the time dimension $\mathbf{y}_a$ $(K_B \times 1)$ is given by

$$\begin{aligned} \mathbf{y}_a = \frac{1}{N_B}\sum_{n=1}^{N_B}\mathbf{y}_n = \frac{1}{N_B}\sum_{n=1}^{N_B}\mathbf{v}_n + \\ + h\left(\sqrt{P_p}\mathbf{g}_p p + \sqrt{P_d}\mathbf{g}_d \circ \left(\frac{1}{N_B}\sum_{n=1}^{N_B}\mathbf{F}_{K_B}\mathbf{d}_n\right)\right), \end{aligned} \tag{10}$$

Then, applying the Least Squares (LS) method [19] and assuming the conditions described in (8) and (9), the estimated channel $\widehat{\mathbf{h}}$ $(K_B \times 1)$ can be obtained as

$$\begin{aligned} \left[\widehat{\mathbf{h}}\right]_k = h\left(1 + \frac{\sqrt{P_d}\,[\mathbf{g}_d]_k}{\sqrt{P_p}\,[\mathbf{g}_p]_k\, p}\frac{1}{N_B}\sum_{n=1}^{N_B}\mathbf{F}_{K_B}\mathbf{d}_n\right) + \\ + \frac{1}{\sqrt{P_p}\,[\mathbf{g}_p]_k\, p}\frac{1}{N_B}\sum_{n=1}^{N_B}\mathbf{v}_n, \end{aligned} \tag{11}$$

and its corresponding mean squared error (MSE) per subcarrier can be derived as

$$\sigma^2_{\Delta h,k} = \frac{1}{N_B P_p \left|[\mathbf{g}_p]_k\right|^2}\left(P_d\left|[\mathbf{g}_d]_k\right|^2 + \sigma_v^2\right). \tag{12}$$

Unlike [14]–[17], the MSE is different for each subcarrier due to the fact that both prototype filter and pilot-pouring coefficients have not the same value for each subcarrier.

Regarding [18], in order to improve the quality of the estimated channel, an additional weighted average in the frequency dimension can be realized. Hence, the estimated channel for the unit block can be obtained as

$$\widehat{h} = \mathbf{w}^T\widehat{\mathbf{h}}, \quad ||\mathbf{w}||_1 = 1, \quad 0 \leq [\mathbf{w}]_k \leq 1, \tag{13}$$

where $\mathbf{w}$ $(K_B \times 1)$ is the vector of weights, and its corresponding MSE can be derived as

$$\sigma^2_{\Delta h} = \frac{1}{N_B P_p}\sum_{k=1}^{K_B}\frac{([\mathbf{w}]_k)^2}{\left|[\mathbf{g}_p]_k\right|^2}\left(P_d\left|[\mathbf{g}_d]_k\right|^2 + \sigma_v^2\right). \tag{14}$$

Before performing the equalization of the received data symbols, the superimposed pilot symbols are removed as follows

$$\mathbf{y}_{d,n} = \mathbf{y}_n - \widehat{h}\left(\sqrt{P_p}\mathbf{g}_p p\right) = \mathbf{h} \circ \sqrt{P_d}\mathbf{g}_d \circ \mathbf{F}_{K_B}\mathbf{d}_n + \tilde{\mathbf{v}}_n, \tag{15}$$

$$\tilde{\mathbf{v}}_n = \left(h - \widehat{h}\right)\sqrt{P_p}\mathbf{g}_p p + \mathbf{v}_n, \tag{16}$$

where $\mathbf{v}_n$ is the additional error term induced by ST [14], and its corresponding error variance can be obtained as

$$\sigma^2_{\tilde{v},k} = P_p\left|[\mathbf{g}_p]_k\right|^2\sigma^2_{\Delta h} + \sigma_v^2. \tag{17}$$

Then, $\mathbf{y}_{d,n}$ is equalized by compensating the effects produced by both the channel ($\widehat{h}$) and the filter coefficients of the data symbols ($\mathbf{g}_d$) in the frequency domain. According to [10]–[12], minimum mean squared error (MMSE) criteria is chosen to avoid the noise enhancement in the edge subcarriers of the RB. Hence it can be expressed as

$$\mathbf{z}_{d,n} = \left(\widehat{h}\mathbf{g}_p + \sigma_v^2\right)^{-1} \circ \mathbf{y}_{d,n}, \tag{18}$$

Finally, an IFFT of size K_B is performed and the decision is made to obtain $\widehat{\mathbf{d}}_n$.

III. Pilot-Pouring Optimization (PPO)

In PPST [18] there is a design space since several parameters can be chosen: the power allocation factor (β), the pilot-pouring coefficients ($\mathbf{g}_p$) and the average coefficients ($\mathbf{w}$). Therefore, the question is how to choose such parameters so that performance of CB-FMT is maximized. Herein, the solution is obtained by defining an optimization problem whose objective is maximizing the SINR under a total power constraint. To proceed, in the next section the SINR is first derived.

A. SINR and Spectral Efficiency

Following the expression of the SINR given in [14, eq. 20-22] and taking into account (15)-(17), the SINR of the received data symbols at the k-th subcarrier can be derived as

$$\begin{aligned}\rho_k &\approx \frac{P_d \left|[\mathbf{g}_d]_k\right|^2}{\left(P_d \left|[\mathbf{g}_d]_k\right|^2 + P_p \left|[\mathbf{g}_p]_k\right|^2\right)\sigma_{\Delta h}^2 + \sigma_v^2} = \\ &= \frac{(1-\beta)\left|[\mathbf{g}_d]_k\right|^2}{\left((1-\beta)\left|[\mathbf{g}_d]_k\right|^2 + \beta\left|[\mathbf{g}_p]_k\right|^2\right)\sigma_{\Delta h}^2 + \sigma_{v_p}^2}, \\ &1 \le k \le K_B, \quad \sigma_{v_p}^2 = \frac{\sigma_v^2}{P_t}.\end{aligned} \tag{19}$$

Note that the first term of the denominator accounts for the interference produced by the channel estimation error in the equalization stage. This term is also present in PSAM systems and it is linearly scaled according to the allocated power to the data $(1-\beta)\left|[\mathbf{g}_d]_k\right|^2$. The second term is the interference induced by the superimposed pilot sequence and the last term accounts for the AWGN.

The SINR of the K_B subcarriers can be obtained as

$$\rho \approx \sum_{k=1}^{K_B} \frac{(1-\beta)\left|[\mathbf{g}_d]_k\right|^2}{\left((1-\beta)\left|[\mathbf{g}_d]_k\right|^2 + \beta\left|[\mathbf{g}_p]_k\right|^2\right)\sigma_{\Delta h}^2 + \sigma_{v_p}^2}. \tag{20}$$

Inspecting (20), it corresponds to a weighted sum due to the presence of the filter coefficients in the numerator $\left|[\mathbf{g}_d]_k\right|^2$, as a consequence of using well-localized prototype filters in the frequency domain. Thus, the contribution of the SINR from the edge subcarriers is marginal as compared to the middle subcarriers.

Therefore, according to [20], we can define spectral efficiency resorting to the achievable rate under the Gaussian input and Gaussian noise assumption as

$$C \propto \eta \mathbb{E}\left\{\log_2(1+\rho)\right\} \text{ [bps/Hz]}, \tag{21}$$

where η denotes the efficiency coefficient of the system. Note that, (21) is presented as a performance indicator in order to provide a performance comparison among the proposed PPST technique against the existing ones in the literature. In ST-based techniques, the efficiency is always maximum ($\eta = 1$) due to the fact that none of the pilot symbols are exclusively occupying a resource element of the unit block, unlike in PSAM ($\eta < 1$).

B. PPO Problem Statement

Before describing the optimization problem, it is important to introduce an additional constraint which is the maximum allowable power (data plus pilot) for any subcarrier (μ watt), in order to avoid the degradation of the system due to the PAPR issues. Therefore, this restriction is described as

$$\mu \ge (1-\beta) P_t \left|[\mathbf{g}_d]_k\right|^2 + \beta P_t \left|[\mathbf{g}_p]_k\right|^2. \tag{22}$$

According to 4G [3] and 5G [4] standards, the pilot symbols devoted to obtaining the CSI are not allowed to be allocated more power than the data ones. Following this principle, it is assumed that μ can be chosen as

$$\mu = (1-\beta) P_t \left(\max(\mathbf{g}_d)\right)^2, \tag{23}$$

where the maximum allowable power for data and pilot symbols is always lower than the maximum gain of the prototype filter in the frequency domain. Consequently, the power allocated to the poured pilots is constrained to the power left unused by the data ones.

Note that (23) points out that the maximum allowable power is limited to the highest coefficient of the frequency response of the prototype filter.

Hence, the optimization problem can be written as follows

$$\begin{aligned}\max_{\beta,\mathbf{g}_p,\mathbf{w}} \quad & \sum_{k=1}^{K_B} \frac{(1-\beta)\left|[\mathbf{g}_d]_k\right|^2}{\left((1-\beta)\left|[\mathbf{g}_d]_k\right|^2 + \beta\left|[\mathbf{g}_p]_k\right|^2\right)\sigma_{\Delta h}^2 + \sigma_{v_p}^2}, \\ & \sigma_{\Delta h}^2 = \frac{1}{N_B}\sum_{r=1}^{K_B}\left([\mathbf{w}]_r\right)^2 \frac{(1-\beta)\left|[\mathbf{g}_d]_r\right|^2 + \sigma_{v_p}^2}{\beta\left|[\mathbf{g}_p]_r\right|^2}, \\ \text{s.t.} \quad & 0 < \beta < 1, \quad \|\mathbf{w}\|_1 = 1, \quad 0 \le [\mathbf{w}]_k \le 1, \\ & \mu \ge (1-\beta) P_t \left|[\mathbf{g}_d]_k\right|^2 + \beta P_t \left|[\mathbf{g}_p]_k\right|^2 \\ & \left\|\mathbf{g}_p\right\|_F^2 \le 1, \quad 1 \le k \le K_B,\end{aligned} \tag{24}$$

where the optimization problem must be jointly solved for the power sharing coefficient β between data and pilot symbols, the pilot-pouring coefficients $\mathbf{g}_d$, and the weighted average coefficients $\mathbf{w}$ implemented at the receiver (see (14)), so that the SINR of the data block is maximized.

The convexity of (24) with respect to its optimization variables is analysed in Appendix A. Due to the definition of the SINR (ρ), it is enough to show that the individual SINR of each subcarrier ($\rho_k,\ 1 \le k \le K_B$) is convex with respect to the optimization variables. Appendix A shows that the optimization problem is strictly convex with respect to the power of pilot-pouring coefficients ($\mathbf{g}_p$) without any restrictions, while it is not convex with respect to the weighted average coefficients ($\mathbf{w}$). Moreover, it is conditionally convex with respect to the power allocation factor (β) if the power/amplitude of the frequency response of the prototype function is higher than or equal to the power/amplitude of the pilot-pouring coefficient for each subcarrier ($\left|[\mathbf{g}_d]_k\right|^2 \ge \left|[\mathbf{g}_p]_k\right|^2,\ 1 \le k \le K_B$). This issue can be easily circumvented due to the fact that the edge bands of a well-localized prototype filter in the frequency domain are those subcarriers that can violate this restriction, however, they have a marginal contribution to the SINR (ρ) of the system, (see (20)). Hence, even though the optimization problem may be providing a local minimum, it can be ensured that it is close to the global one.

C. Global Optimization based on Evolutionary Computation

The evolutionary computation [21] is a set of global optimization techniques based on mimicking biological evolution. It can be exploited in a wide range of complex non-convex optimization problems when classical optimization techniques are not applicable since the objective function is discontinuous, non-differentiable, stochastic, or highly non-linear. Its

complexity is characterized by the population and generation sizes, where the former denotes all possible solutions to the problem which is evaluated using certain fitness functions in order to generate new descendants, and the latter is the amount of times the population is allowed to evolve. Hence, a greater number of population and generation size will correspond to a higher probability of finding better solutions, at the expense of increasing the complexity in terms of memory and time. Some evolutionary strategies include particle swarm, ant colony and genetic algorithms, among others.

Consequently, (24) can be solved by using a global search optimization technique based on evolutionary computation, especially designed for non-convex optimization problems. In order to ensure that the given solution is near the optimum one, the optimization problem must be extensively evaluated in the subspace built by the three variables $(\beta, \mathbf{g}_p, \mathbf{w})$, which can be obtained by repetitively executing the solver at different initial points. More details are given in Section V.

IV. Low-complexity PPO (LPPO)

PPO has a significant complexity in terms of execution time due to the fact that it is a non-convex optimization problem with respect to the weighted average coefficients. As an alternative, the LPPO method is proposed to accelerate the time required in the optimization process and keep, as far as possible, the overall performance as compared to the PPO.

LPPO splits the overall optimization problem into three interconnected optimization problems, where each optimization problem is responsible for each variable (β, $\mathbf{g}_p$ and $\mathbf{w}$), see (Fig. 2). In order to significantly reduce the complexity induced by the search of the weighted average coefficients, as shown in the previous section, these values are constrained to the well-known arithmetic average, and hence, a low-complexity ordered search is proposed to identify the best set of subcarriers to apply the pilot-pouring. The bisection algorithm is used to obtain the power allocation factor by maximizing the SINR (20). However, the average and pilot-pouring coefficients are obtained by minimizing the MSE of the channel estimation given in (24), and at each step the SINR (20) is improved leading to its optimization. Note that this choice will lead to a negligible performance loss in the SINR due to the fact that the average and pilot pouring coefficients are only placed in the first term of the denominator in the SINR (20). Consequently, reducing the channel estimation error will be equivalent to enhancing the SINR. Moreover, exploiting the expression of the MSE for the channel estimation (14) will allow to efficiently obtain the pilot-pouring coefficients by using the well-known Water-Filling method, and the execution time of ordered search can be accelerated by giving more preference to those subcarriers with the lowest channel estimation error. In summary, the bisection algorithm is applied to determine the power allocation factor (β). Then, the ordered search will provide the best subcarrier candidates for pouring the pilot symbols ($\mathcal{K}_S$). Lastly, the Water-Filling method provides the power allocated for the poured pilot symbols for the chosen subcarriers ($\mathbf{g}_p$). More details and the motivation to use each of them are given in the following subsections.

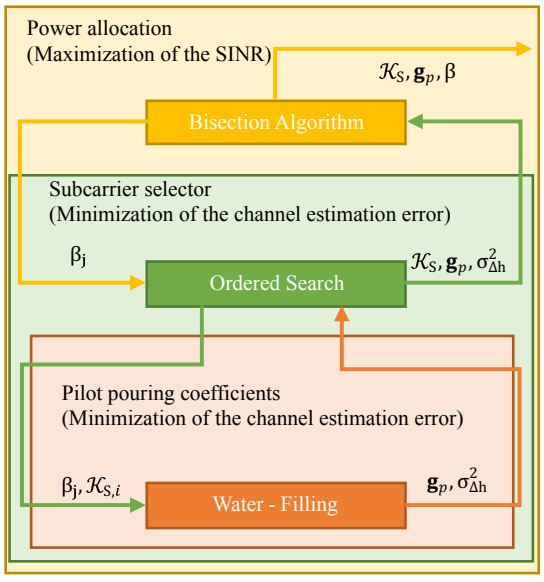

Fig. 2. Block diagram of the LPPO based on interconnected blocks. The top area corresponds to the bisection algorithm, the middle area denotes the ordered search and the bottom area is the Water-Filling method.

A. The Bisection Algorithm

As mentioned in the previous section, the edge subcarriers have a negligible contribution to the SINR of the unit block given in (20), and hence, it is assumed that ρ is convex with respect to the power allocation factor. Consequently, the bisection algorithm [22] is proposed to obtain the best value of β, which is capable of increasing the SINR (20).

The bisection algorithm [22] will provide different values of the power allocation factor for each iteration (β_j, $1 \leq j \leq J$) to the ordered search, where J is the maximum number of allowed iterations for this algorithm (see the top of Fig. 2). Note that J is designed to prevent an infinite loop and it is empirically chosen during the simulation step. For each value of β_j, the ordered search will return a set built by the best set of subcarriers to be exploited for the pilot-pouring, the pilot-pouring coefficients and the channel estimation error ($\mathcal{K}_S$, $\mathbf{g}_p$ and $\sigma^2_{\Delta h}$). The bisection algorithm will obtain the power allocation factor ($\beta \leftarrow \beta_j$) that guarantees the highest SINR.

B. The Ordered Search

According to the previous section, the SINR does not allow a convex optimization with respect to $\mathbf{w}$, and hereby, the complexity of the optimization problem may be excessively high. Furthermore, [18] showed that the minimization of the channel estimation error is able to increase the performance of the system, not only to improve the quality of the channel estimation, but it is also able to reduce the propagation of this error to the data symbols, as shown in (15) and (16). As an alternative to the use of the weighted average coefficients according to (14), an arithmetic average can be used to implement the averaging in the frequency domain. Therefore, the optimization problem consists in obtaining the best set of subcarriers for pouring the pilot symbols for each value of

β_j, capable of minimizing the MSE of the channel estimation error (see the middle of Fig. 2). This is because the arithmetic average corresponds to least square estimation.

This ordered search consists in giving the priority to those edge subcarriers of the RB with very low data power inside. According to (14), the channel estimation error can be lowered if the pilot symbols are mainly poured to those subcarriers that have a very attenuated frequency response coefficient of the prototype filter ($[\mathbf{g}_d]_k \downarrow$), and thus, the number of required evaluations is drastically reduced. Note that, an exhaustive search, which requires $2^{K_B}-1$ iterations, can be also avoided.

Hence, at the i-th iteration, it selects a subset of i subcarriers out of K_B ($\mathcal{K}_{S,i}$) that must satisfy

$$\mathcal{K}_{S,i} \subseteq \mathcal{K}_B, \quad 1 \leq i \leq K_B, \quad \mathcal{K}_{S,i} \neq \emptyset, \quad \left|\mathcal{K}_{S,i}\right| = i. \tag{25}$$

where $\mathcal{K}_B$ denotes the set of K_B subcarriers of the RB, and these i selected subcarriers must satisfy that their corresponding frequency response coefficients of the prototype filter have the lowest power/amplitude of the RB, described as

$$\mathcal{K}_B = \mathcal{K}_{S,i} \cup \mathcal{K}_{S,i}^{\perp}, \quad \mathcal{K}_{S,i} \cap \mathcal{K}_{S,i}^{\perp} = \emptyset, \tag{26}$$

$$\left|[\mathbf{g}_d]_{k_1}\right|^2 \leq \left|[\mathbf{g}_d]_{k_2}\right|^2, \quad \forall k_1 \in \mathcal{K}_{S,i}, \quad \forall k_2 \in \mathcal{K}_{S,i}^{\perp}, \tag{27}$$

where $\mathcal{K}_{S,i}^{\perp}$ denotes the orthogonal set to $\mathcal{K}_{S,i}$. Given the subset of chosen subcarriers at i-th iteration ($\mathcal{K}_{S,i}$) and the β_j provided by the bisection algorithm, the Water-Filling method will provide the pilot-pouring coefficients and the corresponding channel estimation error ($\mathbf{g}_p$ and $\sigma^2_{\Delta h}$). At each iteration of the ordered search, the MSE of the current iteration is compared to the result provided by the previous one. The ordered search will be prematurely interrupted if the channel estimation error has increased from the previous iteration. This means that enabling/selecting more subcarriers for the pilot-pouring does not provide any improvement in terms of channel estimation error. Finally, the indexes of the selected subcarriers at the previous iteration ($\mathcal{K}_S \leftarrow \mathcal{K}_{S,i-1}$) are sent back to the bisection algorithm

C. The Water-Filling method

Given β_j and $\mathcal{K}_{S,i}$ obtained from the previous steps, the main objective is obtaining the best pilot-pouring coefficients $\mathbf{g}_p$ capable of reducing the channel estimation error with a very reduced complexity (see the bottom of Fig. 2). Therefore, the minimization problem can be described as

$$\begin{aligned} \min_{\mathbf{g}_p} \quad & \sum_{k\in\mathcal{K}_{S,i}} \frac{(1-\beta)\left|[\mathbf{g}_d]_k\right|^2 + \sigma^2_{v_p}}{\beta\left|[\mathbf{g}_p]_k\right|^2}, \\ \text{s.t.} \quad & \mu \geq (1-\beta) P_t \left|[\mathbf{g}_d]_k\right|^2 + \beta P_t \left|[\mathbf{g}_p]_k\right|^2, \\ & \left\|\mathbf{g}_p\right\|_F^2 \leq 1, \end{aligned} \tag{28}$$

which is a convex optimization problem. Without taking into account the restriction of maximum allowable power per subcarrier, (28) can be solved by using Lagrange multipliers, where the Lagrange function can be defined as

$$\mathcal{L}\left(\mathbf{g}_p, \lambda\right) = \sum_{k\in\mathcal{K}_{S,i}} \frac{[\mathbf{b}]_k}{\left|[\mathbf{g}_p]_k\right|^2} - \lambda\left(\sum_{k=1}^{K_B}\left|[\mathbf{g}_p]_k\right|^2 - 1\right), \tag{29}$$

$$[\mathbf{b}]_k = \left((1-\beta)\left|[\mathbf{g}_d]_k\right|^2 + \sigma^2_{v_p}\right)\beta^{-1}, \tag{30}$$

and it fulfils the following conditions

$$\frac{\partial\mathcal{L}\left(\mathbf{g}_p,\lambda\right)}{\partial\left|[\mathbf{g}_p]_k\right|^2} = 0 \rightarrow \frac{[\mathbf{b}]_k}{\left(\left|[\mathbf{g}_p]_k\right|^2\right)^2} = -\lambda, \quad k \in \mathcal{K}_{S,i}. \tag{31}$$

From (31), since λ is unique, it follows that

$$\frac{[\mathbf{b}]_{k_1}}{\left(\left|[\mathbf{g}_p]_{k_1}\right|^2\right)^2} = \frac{[\mathbf{b}]_{k_2}}{\left(\left|[\mathbf{g}_p]_{k_2}\right|^2\right)^2}, \quad k_1 \neq k_2, \quad k_1, k_2 \in \mathcal{K}_{S,i}, \tag{32}$$

$$\left|[\mathbf{g}_p]_{k_2}\right|^2 = \left|[\mathbf{g}_p]_{k_1}\right|^2 \sqrt{\frac{[\mathbf{b}]_{k_2}}{[\mathbf{b}]_{k_1}}}, \quad k_1 \neq k_2, \quad k_1, k_2 \in \mathcal{K}_{S,i}. \tag{33}$$

Note that the negative solutions are discarded due to the fact that the power is always a positive value.

Applying (33) to the second constraint in (28), the allocated power for the k_1-th subcarrier can be obtained as

$$\left|[\mathbf{g}_p]_{k_1}\right|^2 \sum_{\substack{k\in\mathcal{K}_{S,i}\\ k\neq k_1}} \sqrt{\frac{[\mathbf{b}]_k}{[\mathbf{b}]_{k_1}}} \leq 1 \rightarrow \left|[\mathbf{g}_p]_{k_1}\right|^2 \leq \left(\sum_{\substack{k\in\mathcal{K}_{S,i}\\ k\neq k_1}} \sqrt{\frac{[\mathbf{b}]_k}{[\mathbf{b}]_{k_1}}}\right)^{-1}. \tag{34}$$

Additionally, in order to fulfil the restriction on the maximum allowable power per subcarrier (μ), the allocated power should be clipped if the allocated power for the poured pilot and data symbols exceeds the limit imposed by μ. Note that, this constraint is established to avoid high power peaks in the frequency domain, and hence, improving the performance of the multi-carrier modulated signal in terms of PAPR. Hence, the power of the pilot-pouring coefficients can be obtained by applying the low-complex Water-Filling technique [23], where the available power is poured at those subcarriers given by $\mathcal{K}_{S,i}$, starting from the edge bands towards the middle band of the unit block.

D. LPPO for high spectrally-shaped prototype filter

For the particular case of exploiting high spectrally-shaped prototype filters for the CB-FMT, the complexity of the proposed LPPO can be further reduced. This particular filter is characterized by having very attenuated frequency responses at both ends of its band, and hence, the potential data interference is also very low and the MSE of the channel estimation is reduced too (see 12). Consequently, it is proposed to exclusively use these two edge subcarriers for the pilot pouring, avoiding the operations required for the ordered search and the Water-Filling method, given in the previous subsections.

Assuming the symmetry property given in (3), the ordered search is replaced by fixing the subcarrier indexes as

$$\mathcal{K}_S = \{1, K_B\}, \tag{35}$$

which are the first and last subcarrier of the RB. The Water-Filling method can be also replaced by fixing the pilot-pouring coefficients as

$$\left|[\mathbf{g}_p]_1\right|^2 = \left|[\mathbf{g}_p]_K\right|^2 = \frac{\beta_j}{2}, \tag{36}$$

TABLE I
PERFORMANCE COMPARISON OF THE DIFFERENT OPTIMIZATION METHODS IN TERMS OF SINR (IN DECIBELS)

	PPO			**LPPO**			**Ref.** [18]		
$\mathbf{K_B}$	**12**	**24**	**36**	**12**	**24**	**36**	**12**	**24**	**36**
SNR = 5 dB	4.31	4.56	4.62	4.29	4.51	4.61	3.78	3.95	4.13
SNR = 10 dB	9.34	9.49	9.67	9.31	9.48	9.61	8.32	8.54	8.97
SNR = 15 dB	14.2	14.49	14.58	14.11	14.41	14.49	12.96	13.12	13.54
SNR = 20 dB	19.28	19.51	19.55	19.19	19.37	19.48	18.15	18.38	18.67

TABLE II
EXECUTION TIME COMPARISON FOR THE DIFFERENT OPTIMIZATION METHODS

	PPO			**LPPO**			**LPPO** (only β opt.)
$\mathbf{K_B}$	**12**	**24**	**36**	**12**	**24**	**36**	**Any**
SNR = 5 dB	31.29 s	33.38 s	37.19 s	9.94 ms	3.19 ms	1.88 ms	1.54 ms
SNR = 10 dB	27.43 s	31.51 s	34.13 s	4.36 ms	1.65 ms	1.57 ms	1.34 ms
SNR = 15 dB	26.51 s	31.49 s	32.42 s	2.72 ms	1.58 ms	1.44 ms	1.12 ms
SNR = 20 dB	25.77 s	27.91 s	30.17 s	1.59 ms	1.46 ms	1.35 ms	0.69 ms

where the total amount of power devoted to pilot symbols at the j-th iteration of the bisection algorithm is equally split by these two subcarriers. Therefore, LPPO is reduced to only finding out the optimum value for β through the bisection algorithm.

V. PERFORMANCE EVALUATION

In this section, we will provide several numerical results in order to show the performance of PPST for the different proposed optimization methods.

Regarding the simulation parameters, the size of the FFT is $K = 1024$, the size of the unit block is $N_B = 14$ and $K_B = \{12, 24, 36\}$. The available power for both data and pilot symbols is normalized to $P_t = 1$. The SNR is defined as SNR $= 1/\sigma_v^2$. Similarly to [10]–[12], the raised-cosine filter is adopted as the prototype filter ($\mathbf{g}_d$), where its roll-off factor is set to $\alpha = 0.2$. The experiments are evaluated using Matlab 2020a, where PPO is implemented by using the Global Optimization Toolbox and specifically the Genetic Algorithm [24] is chosen. The maximum number of execution times for different initial points is set to 100. However, the execution will be stopped as soon as the results keep the same values for the last 10 iterations, in order to prevent an overhead.

A. SINR comparison

In Table I, the performance comparison among the different optimization methods in terms of SINR is given. The numerical results show that PPO provides the best performance for any scenario due to the fact that the provided degrees of freedom to the three variables guarantee the best performance in terms of SINR. However, the performance of the LPPO is slightly lower than PPO at the expense of reducing the complexity, as it is shown in the next subsection. Both proposals outperform the results attained by the reference case given in [18]. Moreover, note that the SINR performance is also slightly improved when the number of subcarriers is incremented. The reason behind this effect is that a higher number of subcarriers provides a higher degree of freedom, and the optimization problem has an additional margin to evaluate more cases.

B. Execution time comparison

The two proposed optimization methods are executed in a PC equipped with an Intel Core i5-7200U at 2.5 Ghz. In Table II, the execution time comparison for the different optimization methods is shown. As already mentioned in the previous subsection, the proposed LPPO has a significant improvement in terms of execution time as compared to the PPO (up to four orders of magnitude), and at the same time it keeps the performance in terms of SINR. The PPO has a high execution time due to the fact that the solver needs to explore many options in the entire subspace produced by the optimization variables, *e.g.* the higher number of subcarriers corresponds to a longer execution time. On the contrary, LPPO has a similar execution time for any value of K_B due to the fact that the ordered search always starts from the edge subcarriers for the pilot allocation, which are the best subcarriers for obtaining the lowest MSE. Moreover, the execution time is higher for low SNR scenarios because more combinations are required to explore. The reason behind this issue is due to the fact that the noise masks the spectrum holes produced by the well-localized prototypes filters in the frequency domain at the edge subcarriers of a RB, and hence, the proposed algorithm requires more time to find out the best solution. Additionally, it also provides the execution time of the LPPO for high spectrally-shaped prototype filter, where only the bisection algorithm is executed. It shows that the execution time is reduced further and it does not depend on the number of subcarriers due to the fact that only the two edge subcarriers are used for pilot-pouring.

C. Illustrative example of pilot-pouring

Two examples of pilot-pouring are given in Figs. 3 and 4 for $K_B = 24$.

Fig. 3 plots an example for a raised-cosine filter with a roll-off factor of $\alpha = 0.2$ and SNR=20 dB. The pilot symbols are exclusively concentrated at the two edge subcarriers of the RB as a consequence of using a high spectrally-shaped prototype filter. Hence, the MSE of the channel estimation can be significantly reduced by using those subcarrier with a lower $\mathbf{g}_d$. When the SNR is lowered, the power of the two pilot symbols will be increased to keep a low MSE. Note that,

a lower MSE also avoids propagating this error to the received data symbols (see 16). This particular scenario asymptotically corresponds to the case of PSAM.

On the other hand, Fig. 4 shows an example for a raise-cosine filter with a roll-off factor of $\alpha = 0.9$ and SNR=10 dB. When the prototype filter is not highly spectrally shaped and the noise power is moderate/high, the two pilot symbols placed at the two edge subcarriers may be not enough to constrain the MSE of the channel estimation, due to the fact that the gain ratio between the middle subcarrier (subcarrier with the highest frequency response) and the two edge subcarriers (subcarriers with the lowest frequency response) is too low. Consequently, the pilot symbols are poured to the contiguous subcarriers, and the averaging factor in the frequency domain will help to reduce the MSE. As an extreme case, the pilot symbols may be uniformly poured to all subcarriers, similarly to the classical ST. Hence, these examples verified that our proposed system is a general case capable of allocating the reference symbols for any case.

D. Spectral efficiency comparison

In Fig. 5, a comparison in terms of spectral efficiency (according to (21)) between PSAM and PPST is given. For the particular scenario of PSAM, the resources devoted to the transmission of reference symbols are obtained from 5G [4], where the demodulation reference symbols (DM-RS) occupy from two to four multi-carrier symbols in a slot ($N_B = 14$). Therefore, the corresponding efficiency is given by $\eta = 2/14$ and $\eta = 4/14$, respectively. The proposed PPST based on both PPO and LPPO not only outperforms PSAM for any value of SNR, but they also exhibit a better performance than the reference case given in [18]. As it can be observed, LPPO exhibits a slight degradation compared to PPO.

In Fig. 6, a comparison in terms of spectral efficiency for different prototype filters (α) and number of subcarriers (K_B) for LPPO is given. The performance for the several configurations is similar due to the fact that the proposed LPPO is always able to maximize the SINR, and hence, the spectral efficiency is increased for any scenario compared to previous works. However, the performance for $K_B = 12$ is slightly worse than for $K_B = 24$ since the number of subcarriers in the pass-band of the prototype filter in the frequency domain is lower in the former case. Additionally, the performance for $\alpha = 0.2$ is better than for $\alpha = 0.9$ given that the power allocated to the poured pilot symbols is higher in the case of $\alpha = 0.9$ (see Fig. 4), and therefore, the spectral efficiency is slightly reduced.

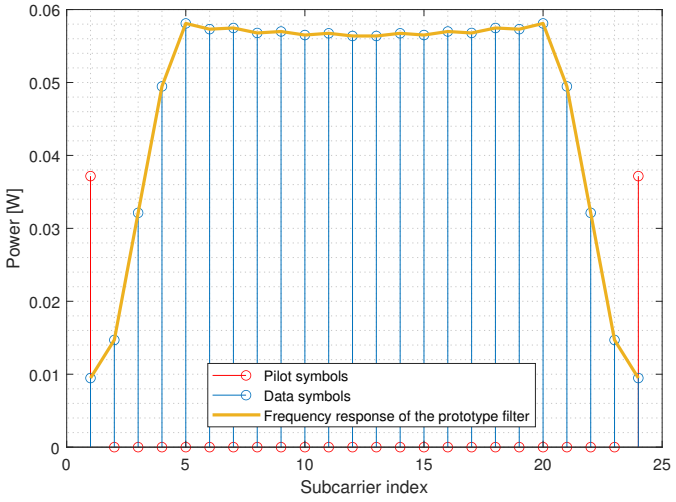

Fig. 3. LPPO for $K_B = 24$, SNR = 20 dBs and $\alpha = 0.2$.

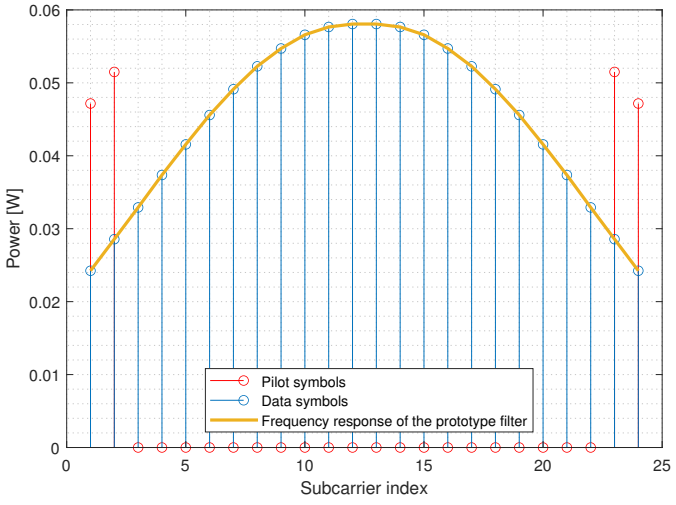

Fig. 4. LPPO for $K_B = 24$, SNR = 10 dBs and $\alpha = 0.9$.

VI. Conclusion

Two optimization solutions are proposed in this work to determine the power allocation in PPST for joint channel estimation and data detection best performance in CB-FMT. The optimized variables is able to increase the spectral efficiency through the SINR optimization taking into account channel estimation using PPST. PPO is able to obtain the best performance due to the fact that none of the variables are constrained, and hence, the provided degree of freedom allows to obtain the highest SINR. On the other hand, LPPO is also proposed to mainly reduce the complexity of PPO and keep the performance as high as possible. The numerical results show the good performance of the proposed algorithms, especially LPPO which can be used in low-latency communications without sacrificing the performance. Additionally, the algorithms and the numerical examples outlined that the proposed optimization problem is a general case of pilot allocation in multi-carrier waveforms, whereas the traditional PSAM and ST are two particular sub-cases.

Appendix A
Analysis of the convexity of the SINR with respect to the pilot-pouring variables

The optimization problem, described (24), is based on the maximization of the SINR with respect to the power allocation factor (β), pilot-pouring coefficients ($\mathbf{g}_p$) and the weighted average coefficients ($\mathbf{w}$). It is relevant to check the concavity of the optimization problem in order to know whether or not a global maximum is available and in which conditions. Due to

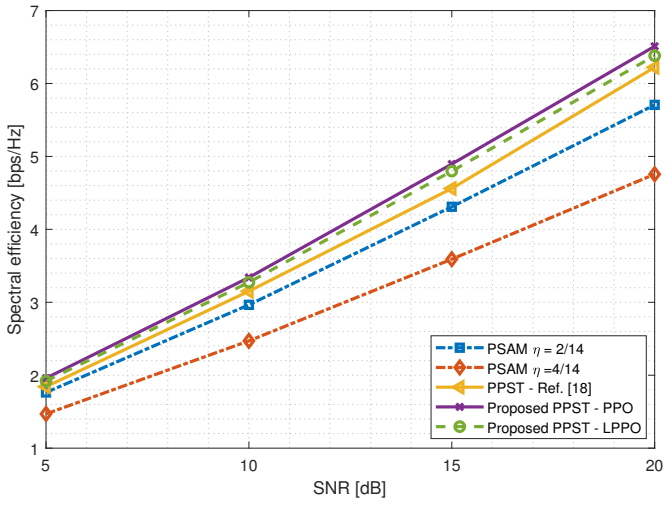

Fig. 5. Comparison of spectral efficiency between PSAM and PPST for $K_B = 36$.

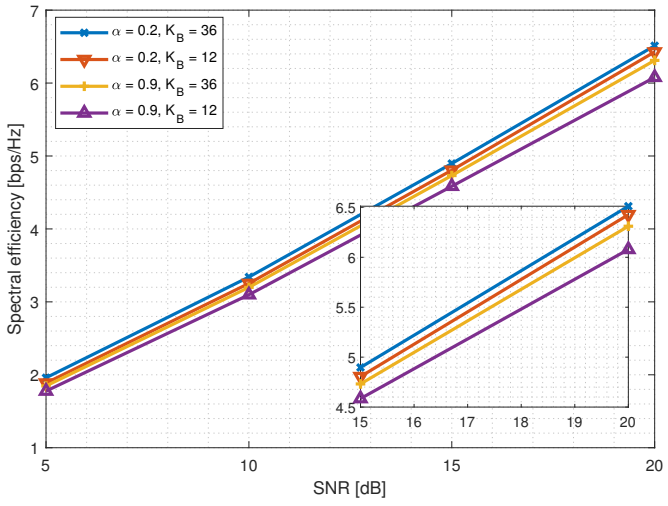

Fig. 6. Comparison of spectral efficiency between different prototype filters and number of subcarriers for LPPO.

the fact that the SINR is an arithmetic average of the individual SINR at each subcarrier (20), it is enough to analyse the convexity of the SINR at each subcarrier (ρ_k, $1 \leq k \leq K_B$) given in (19), which corresponds to verifying that its second derivative with respect to the variable under study is less or equal to zero.

A. Power allocation factor (β)

Firstly, the MSE given in (14) can be rewritten in terms of β as

$$\sigma^2_{\Delta h} = \frac{1-\beta}{\beta}\xi_a + \frac{1}{\beta}\xi_b, \quad \xi_a, \xi_b \geq 0, \tag{37}$$

$$\xi_a = \frac{1}{N_B}\sum_{r=1}^{K_B} \left([\mathbf{w}]_k\right)^2 \frac{\left|[\mathbf{g}_d]_r\right|^2}{\left|[\mathbf{g}_p]_r\right|^2}, \quad \xi_b = \frac{\sigma^2_{v_p}}{N_B}\sum_{k=1}^{K_B} \frac{\left([\mathbf{w}]_r\right)^2}{\left|[\mathbf{g}_p]_r\right|^2}. \tag{38}$$

The first term in the denominator of the SINR (ρ_k) can be expressed as

$$(1-\beta)\left|[\mathbf{g}_d]_k\right|^2 \sigma^2_{\Delta h} = \left|[\mathbf{g}_d]_k\right|^2 \beta^{-1}\left((1-\beta)^2\xi_a + (1-\beta)\xi_b\right), \tag{39}$$

while the second and third terms are given by

$$\beta\left|[\mathbf{g}_p]_k\right|^2 \sigma^2_{\Delta h} + \sigma^2_{v_p} = \left|[\mathbf{g}_p]_k\right|^2 ((1-\beta)\xi_a + \xi_b) + \sigma^2_{v_p}. \tag{40}$$

Hence, ρ_k can be rewritten as

$$\rho_k = \frac{\beta(1-\beta)}{\alpha_2\beta^2 + \alpha_1\beta + \alpha_0}\left|[\mathbf{g}_d]_k\right|^2, \tag{41}$$

$$\begin{aligned}
\alpha_2 &= \xi_a\left(\left|[\mathbf{g}_d]_k\right|^2 - \left|[\mathbf{g}_p]_k\right|^2\right),\\
\alpha_1 &= \xi_a\left(\left|[\mathbf{g}_p]_k\right|^2 - 2\left|[\mathbf{g}_d]_k\right|^2\right) + \xi_b\left(\left|[\mathbf{g}_p]_k\right|^2 - \left|[\mathbf{g}_d]_k\right|^2\right),\\
\alpha_0 &= (\xi_a + \xi_b)\left|[\mathbf{g}_d]_k\right|^2 + \sigma^2_{v_p} \geq 0.
\end{aligned} \tag{42}$$

In order to check if ρ_k is convex with respect to β, it must satisfy that

$$\begin{aligned}
&\frac{\partial^2\rho_k}{\partial\beta^2} \leq 0 \rightarrow\\
&\rightarrow \alpha_2(\alpha_2+\alpha_1)\beta^3 - 3\alpha_2\alpha_0\beta(1-\beta) - \alpha_0(\alpha_1+\alpha_0) \leq 0,
\end{aligned} \tag{43}$$

where this inequality can be satisfied if $\left|[\mathbf{g}_d]_k\right|^2 \geq \left|[\mathbf{g}_p]_k\right|^2$ for the range $(0 < \beta < 1)$.

B. Pilot-pouring coefficients ($\mathbf{g}_p$)

Again, the MSE given in (14) can be rewritten in terms of $\mathbf{g}_p$ as

$$\begin{aligned}
\sigma^2_{\Delta h} = &\frac{1}{N_B}\left([\mathbf{w}]_k\right)^2 \frac{(1-\beta)\left|[\mathbf{g}_d]_k\right|^2 + \sigma^2_{v_p}}{\beta\left|[\mathbf{g}_p]_k\right|^2} +\\
&+ \frac{1}{N_B}\sum_{\substack{v=1\\ v\neq k}}^{K_B}\left([\mathbf{w}]_v\right)^2 \frac{(1-\beta)\left|[\mathbf{g}_d]_v\right|^2 + \sigma^2_{v_p}}{\beta\left|[\mathbf{g}_p]_v\right|^2}.
\end{aligned} \tag{44}$$

The second and third terms in the denominator of the SINR (ρ_k) can be obtained as

$$\beta\left|[\mathbf{g}_p]_k\right|^2 \sigma^2_{\Delta h} + \sigma^2_{v_p} = \xi_c\left|[\mathbf{g}_p]_k\right|^2 + \xi_d + \sigma^2_{v_p}, \tag{45}$$

$$\xi_c = \frac{1}{N_B}\sum_{\substack{v=1\\ v\neq k}}^{K_B}\left([\mathbf{w}]_v\right)^2 \frac{(1-\beta)\left|[\mathbf{g}_d]_v\right|^2 + \sigma^2_{v_p}}{\left|[\mathbf{g}_p]_v\right|^2} \geq 0, \tag{46}$$

$$\xi_d = \frac{1}{N_B}\left([\mathbf{w}]_k\right)^2\left((1-\beta)\left|[\mathbf{g}_d]_k\right|^2 + \sigma^2_{v_p}\right) \geq 0, \tag{47}$$

where ξ_c accounts for the channel estimation error produced by other subcarriers and ξ_d denotes the channel estimation error produced by the k-th subcarrier of interest. Besides, the first term is given by

$$(1-\beta)\left|[\mathbf{g}_d]_k\right|^2 \sigma^2_{\Delta h} = \frac{1-\beta}{\beta}\left|[\mathbf{g}_d]_k\right|^2\left(\frac{\xi_d}{\left|[\mathbf{g}_p]_k\right|^2} + \xi_c\right). \tag{48}$$

Hence, ρ_k can be rewritten as

$$\rho_k = \frac{\left|\left[\mathbf{g}_p\right]_k\right|^2}{\alpha_2\left(\left|\left[\mathbf{g}_p\right]_k\right|^2\right)^2 + \alpha_1\left|\left[\mathbf{g}_p\right]_k\right|^2 + \alpha_0}(1-\beta)\left|\left[\mathbf{g}_d\right]_k\right|^2, \tag{49}$$

$$\alpha_2 = \xi_c, \quad \alpha_1 = \sigma_{v_p}^2 + \xi_d + \xi_c\frac{1-\beta}{\beta}\left|\left[\mathbf{g}_d\right]_k\right|^2, \quad \alpha_0 = \xi_d\frac{1-\beta}{\beta}\left|\left[\mathbf{g}_d\right]_k\right|^2. \tag{50}$$

In order to check if ρ_k is convex with respect to $\left|\left[\mathbf{g}_p\right]_k\right|^2$, it must satisfy that

$$\frac{\partial^2\rho_k}{\partial\left(\left|\left[\mathbf{g}_p\right]_k\right|^2\right)^2} \leq 0 \rightarrow \rightarrow \alpha_2^2\left(\left|\left[\mathbf{g}_p\right]_k\right|^2\right)^3 - 3\alpha_2\alpha_0\left|\left[\mathbf{g}_p\right]_k\right|^2 - \alpha_1\alpha_0 \leq 0, \tag{51}$$

where the inequality holds considering that $0 \leq \left|\left[\mathbf{g}_p\right]_k\right|^2 \leq 1$.

C. Weighted average coefficients ($\mathbf{w}$)

Analogously to the previous subsection and taking into account the expression of the channel estimation error given in (44), the SINR (ρ_k) can be rewritten as

$$\rho_k = \frac{1}{\alpha_1\left(\left[\mathbf{w}\right]_k\right)^2 + \alpha_0}(1-\beta)\left|\left[\mathbf{g}_d\right]_k\right|^2, \tag{52}$$

$$\alpha_1 = \left((1-\beta)\left|\left[\mathbf{g}_d\right]_k\right|^2 + \beta\left|\left[\mathbf{g}_p\right]_k\right|^2\right) \times \times \frac{(1-\beta)\left|\left[\mathbf{g}_d\right]_k\right|^2 + \sigma_{v_p}^2}{N_B\beta\left|\left[\mathbf{g}_p\right]_k\right|^2} \geq 0, \tag{53}$$

$$\alpha_0 = \sigma_{v_p}^2 + \left((1-\beta)\left|\left[\mathbf{g}_d\right]_k\right|^2 + \beta\left|\left[\mathbf{g}_p\right]_k\right|^2\right) \times \times \sum_{\substack{v=1\\v\neq k}}^{K_B}\left(\left[\mathbf{w}\right]_v\right)^2\frac{(1-\beta)\left|\left[\mathbf{g}_d\right]_v\right|^2 + \sigma_{v_p}^2}{N_B\beta\left|\left[\mathbf{g}_p\right]_v\right|^2} \geq 0, \tag{54}$$

where α_1 accounts for the interference produced by the k-th subcarrier of interest and α_0 is the noise plus the interferences produced by the remaining $K-1$ subcarriers.

In order to check if ρ_k is convex with respect to $\left[\mathbf{w}\right]_k$, it must satisfy that

$$\frac{\partial^2\rho_k}{\partial\left[\mathbf{w}\right]_k} \leq 0 \rightarrow 3\alpha_1\left(\left[\mathbf{w}\right]_k\right)^2 - \alpha_0 \leq 0, \tag{55}$$

where this inequality does not hold unless either the noise power is excessively high or all other subcarriers are disabled, and both situations correspond to unrealistic cases.

REFERENCES

[1] T. Hwang, C. Yang, G. Wu, S. Li, and G. Y. Li, "OFDM and its wireless applications: A survey," *IEEE Transactions on Vehicular Technology*, vol. 58, no. 4, pp. 1673–1694, May 2009.

[2] Jun Cai, Xuemin Shen, and J. W. Mark, "Robust channel estimation for OFDM wireless communication systems," *IEEE Transactions on Wireless Communications*, vol. 3, no. 6, pp. 2060–2071, Nov. 2004.

[3] "Evolved universal terrestrial radio access (E-UTRA); physical channels and modulation," 3GPP, France, Technical Report 36.211, 2017.

[4] "NR; Physical channels and modulation (Release 16)," 3GPP, France, Technical Report 38.211, 2020.

[5] G. Cherubini, E. Eleftheriou, and S. Olcer, "Filtered multitone modulation for very high-speed digital subscriber lines," *IEEE Journal on Selected Areas in Communications*, vol. 20, no. 5, pp. 1016–1028, June 2002.

[6] L. Zhang, P. Xiao, A. Zafar, A. u. Quddus, and R. Tafazolli, "FBMC system: An insight into doubly dispersive channel impact," *IEEE Transactions on Vehicular Technology*, vol. 66, no. 5, pp. 3942–3956, May 2017.

[7] H. Nam, M. Choi, S. Han, C. Kim, S. Choi, and D. Hong, "A new filter-bank multicarrier system with two prototype filters for QAM symbols transmission and reception," *IEEE Transactions on Wireless Communications*, vol. 15, no. 9, pp. 5998–6009, Sep. 2016.

[8] X. Chen, L. Wu, Z. Zhang, J. Dang, and J. Wang, "Adaptive modulation and filter configuration in universal filtered multi-carrier systems," *IEEE Transactions on Wireless Communications*, vol. 17, no. 3, pp. 1869–1881, March 2018.

[9] D. Zhang, A. Festag, and G. P. Fettweis, "Performance of generalized frequency division multiplexing based physical layer in vehicular communications," *IEEE Transactions on Vehicular Technology*, vol. 66, no. 11, pp. 9809–9824, Nov. 2017.

[10] A. M. Tonello and M. Girotto, "Cyclic block filtered multitone modulation," *EURASIP Journal on Advances in Signal Processing*, vol. 109, July 2014.

[11] M. Girotto and A. M. Tonello, "Orthogonal design of cyclic block filtered multitone modulation," *IEEE Transactions on Communications*, vol. 64, no. 11, pp. 4667–4679, Nov. 2016.

[12] N. Moret and A. M. Tonello, "Design of orthogonal filtered multitone modulation systems and comparison among efficient realizations," *EURASIP Journal on Advances in Signal Processing*, vol. 141865, Feb. 2010.

[13] M. K. Tsatsanis and Zhengyuan Xu, "Pilot symbol assisted modulation in frequency selective fading wireless channels," *IEEE Transactions on Signal Processing*, vol. 48, no. 8, pp. 2353–2365, Aug. 2000.

[14] W. Huang, C. Li, and H. Li, "On the power allocation and system capacity of OFDM systems using superimposed training schemes," *IEEE Transactions on Vehicular Technology*, vol. 58, no. 4, pp. 1731–1740, May 2009.

[15] K. Chen-Hu, J. C. Estrada-Jimenez, M. J. Fernandez-Getino Garcia, and A. G. Armada, "Superimposed training for channel estimation in FBMC-OQAM," in *2017 IEEE 86th Vehicular Technology Conference (VTC-Fall)*, Sep. 2017, pp. 1–5.

[16] J. C. Estrada-Jiménez, K. Chen-Hu, M. J. F. García, and A. García Armada, "Power allocation and capacity analysis for FBMC-OQAM with superimposed training," *IEEE Access*, vol. 7, pp. 46 968–46 976, 2019.

[17] J. C. Estrada-Jiménez and M. J. Fernández-Getino García, "Partial-data superimposed training with data precoding for OFDM systems," *IEEE Transactions on Broadcasting*, vol. 65, no. 2, pp. 234–244, June 2019.

[18] K. Chen-Hu, M. Julia Fernández-Getino García, A. M. Tonello, and A. G. Armada, "Pilot pouring in superimposed training for channel estimation in CB-FMT," *IEEE Transactions on Wireless Communications*, pp. 1–1, 2021.

[19] J. Lin, "Least-squares channel estimation for mobile OFDM communication on time-varying frequency-selective fading channels," *IEEE Transactions on Vehicular Technology*, vol. 57, no. 6, pp. 3538–3550, Nov. 2008.

[20] Shuichi Ohno and G. B. Giannakis, "Capacity maximizing MMSE-optimal pilots for wireless OFDM over frequency-selective block rayleigh-fading channels," *IEEE Transactions on Information Theory*, vol. 50, no. 9, pp. 2138–2145, Sep. 2004.

[21] A. N. Sloss and S. Gustafson, *2019 Evolutionary Algorithms Review*. Cham: Springer International Publishing, 2020, pp. 307–344.

[22] C. Clapham and J. Nicholson, *The Concise Oxford Dictionary of Mathematics*, 4th ed. Oxford University Press, 2009.

[23] P. He and L. Zhao, "Noncommutative composite water-filling for energy harvesting and smart power grid hybrid system with peak power constraints," *IEEE Transactions on Vehicular Technology*, vol. 65, no. 4, pp. 2026–2037, April 2016.

[24] R. R. Bies, M. F. Muldoon, B. G. Pollock, S. Manuck, G. Smith, and M. E. Sale, "A genetic algorithm-based, hybrid machine learning approach to model selection," *Journal of Pharmacokinetics and Pharmacodynamics*, vol. 33, p. 95.221, 2006.

Kun Chen-Hu (S'16-GS'20-M'21) received his Ph.D. degree in Multimedia and Communications in 2019 from Universidad Carlos III de Madrid (Spain). Currently, he is a post-doctoral researcher in the same institution. He was awarded by UC3M in 2019 recognizing his outstanding professional career after graduation. He visited Eurecom (France) and Vodafone Chair TU Dresden (Germany), both as guest researcher. He also participated in different research projects in collaboration with several top companies in the area of mobile communications. He is the Web Chair for Globecom 2021, Madrid (Spain), and online content editor for IEEE ComSoc. His research interests are related to signal processing techniques, such as waveforms design, reconfigurable intelligent surfaces, non-coherent massive MIMO and channel estimation.

M. Julia Fernández-Getino García (S'99 - AM'02 - M'03) received the M. Eng. and Ph.D. degrees in telecommunication engineering from the Polytechnic University of Madrid, Spain, in 1996 and 2001, respectively. She is currently with the Department of Signal Theory and Communications, Carlos III University of Madrid, Spain, as an Associate Professor. From 1996 to 2001, she held a research position with the Department of Signals, Systems and Radiocommunications, Polytechnic University of Madrid. She visited Bell Laboratories, Murray Hill, NJ, USA, in 1998; visited Lund University, Sweden, during two periods in 1999 and 2000; visited Politecnico di Torino, Italy, in 2003 and 2004; and visited Aveiro University, Portugal, in 2009 and 2010. Her research interests include multicarrier communications, coding and signal processing for wireless systems.

She received the best "Master Thesis" and "Ph.D. Thesis" awards from the Professional Association of Telecommunication Engineers of Spain in 1998 and 2003, respectively; the "Student Paper Award" at the IEEE International Symposium on Personal, Indoor and Mobile Radio Communications (PIMRC) in 1999; the "Certificate of Appreciation" at the IEEE Vehicular Technology Conference (VTC) in 2000; the "Ph.D. Extraordinary Award" from the Polytechnic University of Madrid in 2004; the "Juan de la Cierva National Award" from AENA Foundation in 2004; and the "Excellence Award" from Carlos III University of Madrid in 2012 for her research career.

Andrea M. Tonello (M'00-SM'12) received the Laurea degree (summa cum laude) in electrical engineering and the Doctor of Research degree in electronics and telecommunications from the University of Padova, Padua, Italy, in 1996 and 2002, respectively. From 1997 to 2002, he was with Bell Labs-Lucent Technologies, Whippany, NJ, USA, first as a Member of the Technical Staff. He was then promoted to Technical Manager and appointed as the Managing Director of the Bell Labs, Italy Division. In 2003, he joined the University of Udine, Udine, Italy, where he became an Aggregate Professor, in 2005 and an Associate Professor, in 2014. He is currently a Professor with the Chair of Embedded Communication Systems, University of Klagenfurt, Klagenfurt, Austria. He received several awards, including the Bell Labs Recognition of Excellence Award (1999), the Distinguished Visiting Fellowship from the Royal Academy of Engineering, U.K. (2010), the IEEE Distinguished Lecturer Award from VTS (2011-15) and from COMSOC (2018-19), the Italian Full Professor Habilitation (2013), the Chair of Excellence from Carlos III Universidad, Madrid (2019-20). He was also a co-recipient of nine best paper awards. He serves/ed as associate editor of several journals, including IEEE TVT, IEEE TCOM, IEEE ACCESS, and IET Smart Grid. He was the general chair or TPC co-chair of several conferences. He was the chair of the IEEE COMSOC Technical Committee (TC) on Power Line Communications (2014-18) and he is currently the Chair of the TC on Smart Grid Communications. He also serves as Director of Industry Outreach of IEEE COMSOC for the term 2019-20.

Ana García Armada (S'96-A'98-M'00-SM'08) received the Ph.D. degree in electrical engineering from the Polytechnical University of Madrid in February 1998. She is currently a Professor at Universidad Carlos III de Madrid, Spain. She is leading the Communications Research Group at this university. She has participated in more than 30 national and 10 international research projects as well as 20 contracts with the industry. Her research has resulted in 9 book chapters, and more than 150 publications in prestigious international journals and conferences, as well as 5 patents. She has also contributed to standardization organizations (ITU, ETSI) and is a member of the European 5G PPP Group of Experts, as well as the Spanish representative in the committee of the ESA Joint Board on Communication Satellite Programs 5G Advisory Committee (5JAC). She has been Editor (2016–2019, Exemplary Editor Award 2017 and 2018) and Area Editor (2019-2020, Exemplary Editor Award 2020) of IEEE Communication Letters. She is Editor of IEEE Transactions on Communications since 2019, Area Editor of IEEE Open Journal of the Communications Society since 2019, Editor of the ITU Journal on Future and Evolving Technologies and is a regular member of the technical program committees of the most relevant international conferences in his field. She has formed / is part of the organizing committee of the IEEE Globecom 2019 and 2021 (General Chair), IEEE Vehicular Technology Conference Spring 2018, 2019 and Fall 2018, IEEE 5G Summit 2017, among others. She is Secretary of the IEEE ComSoc Signal Processing and Computing for Communications Committee, has been Secretary and Chair of the IEEE ComSoc Women in Communications Engineering Standing Committee. Since January 2020 she is Director of Online Content of the IEEE Communications Society. She has received the Award of Excellence from the Social Council and the Award for Best Teaching Practices from Universidad Carlos II de Madrid, as well as the third place Bell Labs Prize 2014, the Outstanding Service Award 2019 from the SPCE committee of the IEEE Communications Society and the Outstanding Service Award 2020 from the Women in Communications Engineering (WICE) standing committee.